

# Proton elastic scattering from light nuclei at low and intermediate energies using microscopic optical model and the eikonal approximation

Hasan Maridi

18 March 2021

Heavy ion Laboratory, University of Warsaw, Poland  
under the grant of the Ulam Programme from the Polish National  
Agency for Academic Exchange (NAWA)

For Online Seminars in Faculty of Physics, University of Warsaw

# 1-a Proton elastic scattering of light nuclei I

- The system of the elastic scattering can be approximated by considering the complex optical model potential.
- In the phenomenological approach, a suitable analytical forms as a Woods-Saxon or Gaussian forms are used with free parameters which are adjusted to best fit with available experimental data.
- In microscopic approach, as the folding model, the nucleon-nucleon interaction and the matter distributions of the colliding nuclei are considered.
- For weakly bound nuclei, the folding potential requires a normalization to fit the data indicating to the breakup effect.

# Proton elastic scattering of light nuclei I

The most important goals of the present work are:

- To use a minimal number of fitting parameters in the OP.
  - To determine the energy dependencies of the OP.
  - To present an energy-dependent local microscopic OP which can be used to predict the data at energies where no experimental data are available.
- 
- The proton elastic scattering data of the light nuclei,  ${}^4,6,8\text{He}$ ,  ${}^{6,7,9,11}\text{Li}$ , and  ${}^{9,10,11,12}\text{Be}$ , in the range of few MeVs/nucleon to 200 MeV/nucleon is studied.
  - The cross-section data are calculated by the optical model analysis with partial-wave expansion method.
  - The OP is constructed only from the single-folding model and its derivative

# Proton elastic scattering of light nuclei II

$d\sigma/d\Omega$  and  $A_y(\theta)$  data for proton elastic scattering of helium, lithium, and beryllium isotopes from 1964 to 2013.

| Data                    | Scattering   | Incident energy (MeV/nucleon)  |
|-------------------------|--|--|
| $d\sigma/d\Omega$       | $p+{}^4\text{He}$  | 12.04, 17.45, 31.0, 40, 45, 64.9, 71.9, 85, and 156                              |
|                         | ${}^6\text{He}+p$  | 25.1, 38.3, 40.9, 41.6, and 71   |
|                         | ${}^8\text{He}+p$  | 15.7, 26.1, 32, 66, and 72   |
|                         | $p+{}^6\text{Li}$  | 6.0, 10.0, 25.9, 29.9, 35, 40.1, 45.4, 49.75, 65, 72, 135, 155, and 200.4        |
|                         | $p+{}^7\text{Li}$  | 6.15, 10.3, 24.4, 49.74, 65, 155, and 200.4                                      |
|                         | ${}^{9,11}\text{Li}+p$   | 60 for ${}^9\text{Li}+p$ ; 62, 68.4, and 75 for ${}^{11}\text{Li}+p$             |
|                         | $p+{}^9\text{Be}$  | 3, 6, 10, 13, 30.3, 17, 25, 35.2, 49.4, 54.7, 74.7, 100.6, 160, 179.9, and 201.4 |
|                         | ${}^{10}\text{Be}+p$   | 6, 9, 12, 15, 39.1, and 59.3   |
| ${}^{11,12}\text{Be}+p$ | 38.4 and 49.3 for ${}^{11}\text{Be}+p$ and 55 for ${}^{12}\text{Be}+p$ . |  |
| $A_y(\theta)$           | $p+{}^4\text{He}$  | 8.5, 14.5, 45, 52.3, 59.6, 64.9, and 71.9  |
|                         | ${}^{6,8}\text{He}+p$  | 71 for ${}^6\text{He}+p$ and 72 for ${}^8\text{He}+p$                            |
|                         | $p+{}^6\text{Li}$  | 10, 14.5, 65, 72   |
|                         | $p+{}^7\text{Li}$  | 14.5, 65   |
|                         | $p+{}^9\text{Be}$  | 8.5, 11.4, 13, 17.8, 30.3, 42, 74.7, 100.6                                       |

- The total optical potential  $U_{OP}(r)$  can be generally written as

$$U_{OP}(r) = V_N(r) + V_{SO}(r)\mathbf{L}\cdot\mathbf{S} + V_C(r), \quad (1)$$

where  $V_N(r) = V(r) + iW(r)$  is the complex nuclear potential,  $V_{SO}$  is the spin-orbit potential, and  $V_C(r)$  is the Coulomb potential of a uniformly charged sphere.

- The phenomenological optical potential is taken in the popular Woods-Saxon form:

$$U_{OP}(r) = V_C(r) - V_0 f_0(r) - iW_v f_v(r) + 4ia_s W_s \frac{d}{dr} f_s(r) + 2\lambda_{\pi}^2 V_{so} \frac{1}{r} \frac{d}{dr} f_{so}(r), \quad (2)$$

where  $f_x(r) = \left[1 + \exp\left(\frac{r-R_x}{a_x}\right)\right]^{-1}$ ,  $R_x = r_x A^{1/3}$ , with  $A$  being the atomic mass number, and  $\lambda_\pi^2 = \left(\frac{\hbar}{m_\pi c}\right)^2 \approx 2 \text{ fm}^2$ . The subscripts  $x = 0, v, s$ , and so denote the central real, volume imaginary, surface imaginary, and spin-orbit, respectively.  $V_0, W_v(W_s)$  and  $V_{so}$  are the strengths.

- In this work, the microscopic OP can be written as

$$U_{\text{OP}}(r) = N_R V_F(r) + i[N_{\text{IV}} W_F(r) - N_{\text{IS}} r \frac{d}{dr} W_F(r)] - 2\lambda_\pi^2 N_{\text{SO}} \frac{1}{r} \frac{d}{dr} V_F(r) \mathbf{L} \cdot \mathbf{S}. \quad (3)$$

- Renormalization factors are introduced to fit the data.
- The fitting procedure is carried out by:

# Total optical potential III

- simultaneously adjustment of the renormalization factors of the OP to fit the cross-section data.
- is done by achieving a minimum  $\chi^2$

$$\chi^2 = \frac{1}{N} \sum_{k=1}^N \left[ \frac{\sigma_{\text{th}}(\theta_k) - \sigma_{\text{ex}}(\theta_k)}{\Delta\sigma_{\text{ex}}(\theta_k)} \right]^2, \quad (4)$$

- the single-folding potential  $V_F(r)$  is given by

$$\begin{aligned} V_F(r) &= \int \rho(\mathbf{r}') \nu_{nn}(s) d\mathbf{r}', \\ &= \frac{1}{(2\pi)^3} \int d\mathbf{q} e^{-i\mathbf{q}\cdot\mathbf{r}} \tilde{\rho}(\mathbf{q}) \tilde{\nu}_{nn}(\mathbf{q}), \end{aligned} \quad (5)$$

where  $s = |\mathbf{r} - \mathbf{r}'|$ , is the distance between the two nucleons,  $\rho(\mathbf{r}')$  is the density of the nucleus at  $r$ , and  $\nu_{nn}(s)$  is the effective  $NN$  interaction between two nucleons.

# Total optical potential IV

- The parameterized form of the density-independent M3Y-Reid interaction is

$$\nu_{nn}(s) = 7999 \frac{e^{(-4s)}}{4s} - 2134 \frac{e^{(-2.5s)}}{2.5s} - 276(1 - 0.005E/A)\delta(s), \quad (6)$$

where the last term is the zero-range pseudopotential.

- The microscopic densities: large-scale shell model (LSSM and Green's function Monte Carlo GFMC) are used.
- Also, the imaginary part  $W$  within folding model as

$$W_F(r) = \frac{1}{(2\pi)^3} \int d\mathbf{q} e^{-i\mathbf{q}\cdot\mathbf{r}} \tilde{\rho}(\mathbf{q}) \tilde{w}_{nn}(\mathbf{q}), \quad (7)$$

where

$$\tilde{w}_{nn}(\mathbf{q}) = \frac{\hbar v}{2} \bar{\sigma}_{NN} f_{NN}(q), \quad (8)$$



where  $v$  is the velocity of the nucleon-nucleus relative motion,  $\rho(q)$  is the form factor corresponding to the point like nucleon density distribution of the nucleus, and

$f_{NN}(q) = \exp(-q^2 r_0^2/4)$  is the amplitude of the  $NN$  scattering and  $r_0^2 = 0.439 \text{ fm}^2$  is the range parameter.  $\bar{\sigma}_{NN}$  is the averaged over isospin total  $NN$  cross section. It has been parameterized as a function of energy.

## 1-b Local E-dependent microscopic nucleon-nucleus OP I

- There are three methods commonly used to set the parameterization of the OP:
  - ① A best-fit OP: representing a potential for one reaction at one single incident energy.
  - ② a local OP: representing a potential for one reaction and an energy region.
  - ③ a global OP: in which a potential is specified for both a mass region and an energy region
- We present a local E-dependent microscopic OP with parameterized N-factors to reproduce the cross-section data for the nucleon-nucleus scattering of  $p+^{4,6,8}\text{He}$ ,  $p+^{6,7}\text{Li}$ , and  $p+^{9,10}\text{Be}$  at energy range from few MeVs/nucleon up to 200 MeV/nucleon.

# Local E-dependent microscopic nucleon-nucleus OP I

To initialize this E-dependent OP, the following steps are done:

- First, the fitting procedure is carried out to fit  $d\sigma/d\Omega$ ,  $A_y(\theta)$ , and  $\sigma_R$  data using the best-fit microscopic OP

$$U_{\text{OP}}(r) = N_R V_F(r) + i[N_{\text{IV}} W_F(r) - N_{\text{IS}} r \frac{d}{dr} W_F(r)] - 2\lambda_\pi^2 N_{\text{SO}} \frac{1}{r} \frac{d}{dr} V_F(r) \text{L.S.} \quad (9)$$

- Second, the volume integrals of the best-fit OP are calculated

$$J(U) = \frac{4\pi}{A} \int U(r) r^2 dr. \quad (10)$$

$$J_R = \frac{4\pi}{A} \int [N_R V_F(r)] r^2 dr. \quad (11)$$

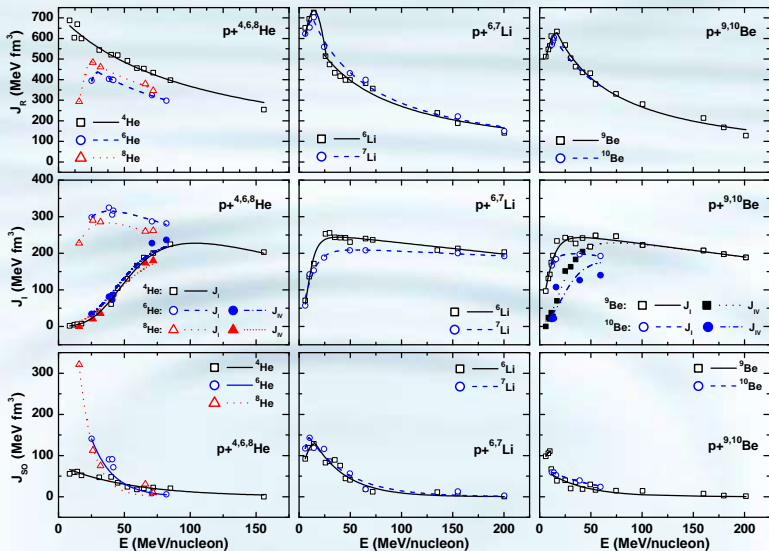
$$J_I = J_{IV} + J_{IS} = \frac{4\pi}{A} \int [N_{IV} W_F(r) - N_{IS} r \frac{d}{dr} W_F(r)] r^2 dr. \quad (12)$$

$$J_{SO} = \frac{4\pi}{A} \int [-2\lambda_\pi^2 N_{SO} \frac{1}{r} \frac{d}{dr} V_F(r)] r^2 dr. \quad (13)$$

where  $J_{IV}$  and  $J_{IS}$  are the volume integral of the volume and surface imaginary potentials.

- **Third**, the calculated volume integrals of the best-fit OP are plotted and parameterized as functions in energies

# Local E-dependent microscopic nucleon-nucleus OP III



- These calculated volume integrals are parameterized as follow:

$$J_R(E) = \begin{cases} J_{R0}/(1 + \eta E) & \text{if } E \geq E_R, \\ J_{R1} \exp[-(E - E_R)^2/w_R^2] & \text{if } E \leq E_R \end{cases} \quad (14)$$

$$J_{SO}(E) = \begin{cases} J_{S0} \exp(-E/\gamma) & \text{if } E \geq E_{SO}, \\ J_{S1} \exp[-(E - E_{SO})^2/w_{SO}^2] & \text{if } E \leq E_{SO} \end{cases} \quad (15)$$

with  $J_{R1} = J_{R0}/(1 + \eta E_R)$  and  $J_{S1} = J_{S0} \exp(-E_{SO}/\gamma)$ . In some cases no data at low energies, so  $E_R$  and  $E_{SO}$  cannot be determined. So, we consider the first line in the equation for  $J_R(E)$  and  $J_{SO}(E)$  for all energies.

$$J_I(E) = (J_{I0} - \alpha_I E) \frac{(E - E_F)^4}{(E - E_F)^4 + \beta_I^4}, \quad (16)$$

$$J_{IV}(E) = (J_{I0} - \alpha_I E) \frac{(E - E_F)^4}{(E - E_F)^4 + \beta_{IV}^4} \quad (17)$$

$$J_{IS}(E) = J_I(E) - J_{IV}(E) = J_I(E) \frac{\beta_{IV}^4 - \beta_I^4}{(E - E_F)^4 + \beta_{IV}^4}. \quad (18)$$

If the imaginary OP is volume only, then  $\beta_{IV} = \beta_I$ .

- The parameters of the volume integral parameterizations are:

| Nucleus          | $E_F$<br>MeV | $E_R$<br>MeV | $w_R$<br>MeV | $J_{R0}$<br>MeV fm <sup>3</sup> | $\eta$<br>MeV <sup>-1</sup> | $J_{I0}$<br>MeV fm <sup>3</sup> | $\alpha_I$<br>MeV <sup>-1</sup> | $\beta_I$<br>MeV | $\beta_{IV}$<br>MeV | $E_{S0}$<br>MeV | $w_{S0}$<br>MeV | $J_{S0}$<br>MeV fm <sup>3</sup> | $\gamma$<br>MeV <sup>-1</sup> |
|------------------|--------------|--------------|--------------|---------------------------------|-----------------------------|---------------------------------|---------------------------------|------------------|---------------------|-----------------|-----------------|---------------------------------|-------------------------------|
| <sup>4</sup> He  | -8.92        |              |              | 694.4                           | 0.0094                      | 293.3                           | 0.386                           | 61.0             | 61.0                |                 |                 | 62.9                            | 108.6                         |
| <sup>6</sup> He  | -16.28       | 25           | 16.6         | 595.2                           | 0.0128                      | 334.1                           | 0.401                           | 20.1             | 72.1                |                 |                 | 434.1                           | 23.7                          |
| <sup>8</sup> He  | -19.13       | 30           | 23.1         | 628.9                           | 0.0111                      | 306.1                           | 0.861                           | 28.6             | 91.1                |                 |                 | 1342.8                          | 10.6                          |
| <sup>6</sup> Li  | -5.10        |              |              | 737.1                           | 0.0180                      | 267.0                           | 0.423                           | 14.6             | 14.6                | 10              | 5.7             | 190.2                           | 41.4                          |
| <sup>7</sup> Li  | -13.62       |              |              | 746.6                           | 0.0173                      | 223.4                           | 0.118                           | 23.1             | 23.1                | 20              | 20.1            | 417.0                           | 29.4                          |
| <sup>9</sup> Be  | -11.74       | 17           | 25.5         | 841.7                           | 0.0222                      | 260.2                           | 0.354                           | 19.1             | 35.9                |                 |                 | 111.3                           | 44.0                          |
| <sup>10</sup> Be | -15.43       |              |              | 714.5                           | 0.0153                      | 215.1                           | 0.490                           | 18.6             | 43.2                |                 |                 | 72.9                            | 56.7                          |

- Finally, the local E-dependent microscopic OP for nucleon-nucleus scattering can be defined as

$$U_{\text{OP}}(r, E) = N_R(E)V_F(r) + i[N_I(E)W_F(r) - N_{\text{IS}}(E)r\frac{d}{dr}W_F(r)] - 2\lambda_{\pi}^2 N_{\text{SO}}(E)\frac{1}{r}\frac{d}{dr}V_F(r)\mathbf{L}\cdot\mathbf{S}. \quad (19)$$

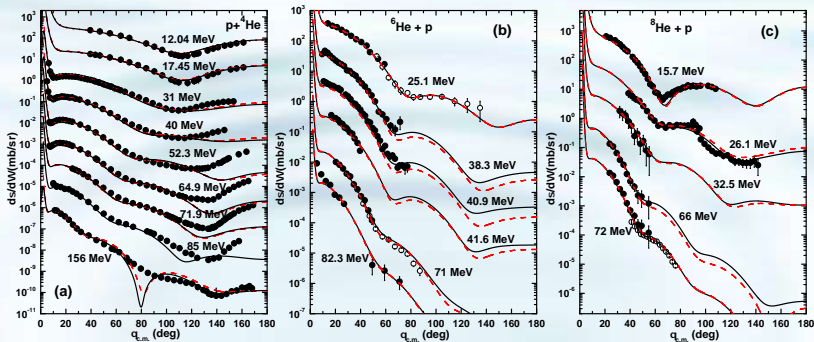
where the parameterized N-factors are defined as:

$$\begin{aligned} N_R(E) &= \frac{J_R(E)}{J(V_F)} \\ N_{\text{IV}}(E) &= \frac{J_{\text{IV}}(E)}{J(W_F)} \\ N_{\text{IS}}(E) &= \frac{J_{\text{IS}}(E)}{J(rdW_F(r)/dr)} \\ N_{\text{SO}}(E) &= \frac{J_{\text{SO}}(E)}{J(2\lambda_{\pi}^2\frac{1}{r}\frac{d}{dr}V_F(r))}. \end{aligned} \quad (20)$$

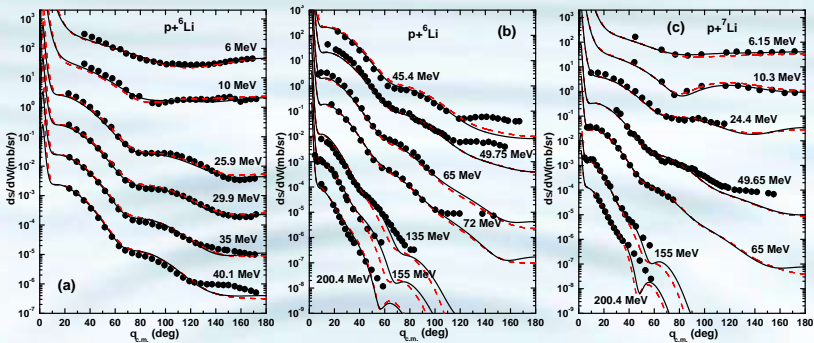


# Local E-dependent microscopic nucleon-nucleus OP VII

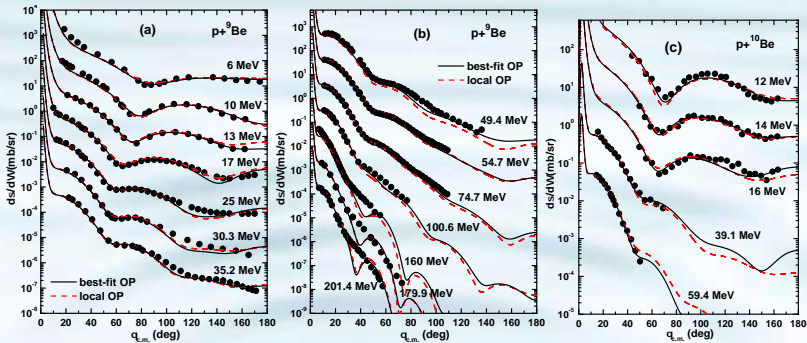
This local OP is applied to analyze the proton elastic scattering of  $4,6,8\text{He}$ ,  $6,7\text{Li}$ , and  $9,10\text{Be}$  nuclei at a wide range of energy from few MeVs/nucleon up to 200 MeV/nucleon.



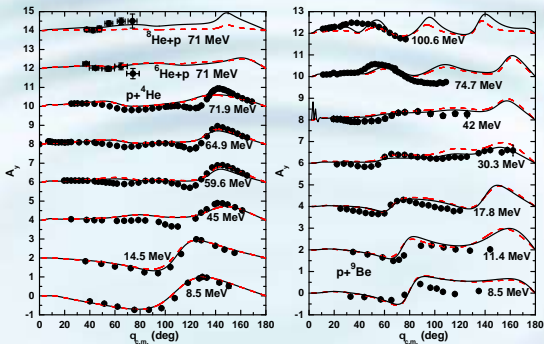
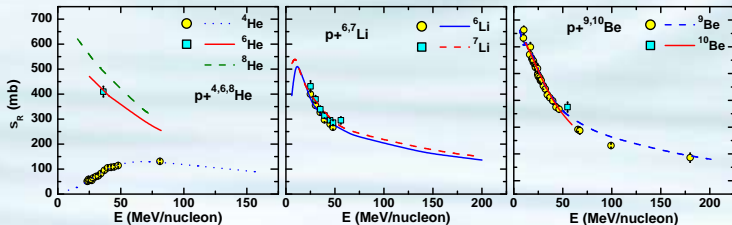
# Local E-dependent microscopic nucleon-nucleus OP VIII



# Local E-dependent microscopic nucleon-nucleus OP IX



# Local E-dependent microscopic nucleon-nucleus OP X

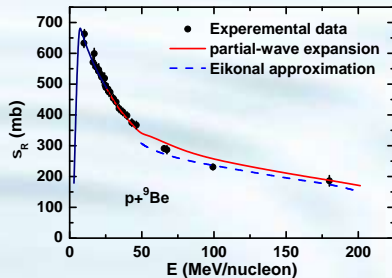
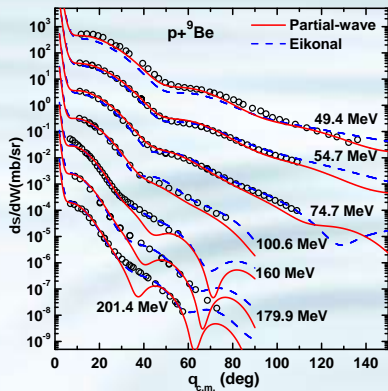


# 1-c Comparing between OM and Eikonal approximation I

In this work

- A comparing between partial wave expansion and eikonal approximation is done for  $p+{}^9\text{Be}$  at energies larger than 50 MeV/nucleon.
- For energies larger than 100 MeV/nucleon, more than one minima are appear in the differential cross-section data using the optical model with the partial-wave expansion method.
- At these energies, the wave function will oscillate rapidly, so, we use the eikonal approximation that based on the Glauber theory with the same OP instead of the partial-wave expansion method.

# Comparing between OM and Eikonal approximation I



The present scattering problem considers a proton with an energy  $E_{\text{Lab}}$  and spin  $s = 1/2$  incident upon a target with mass number  $A$ . It is scattered by a central spherical optical potential  $U = U_{\text{OP}}(r)$  that satisfy the optical Schrödinger equation as

$$\frac{-\hbar^2}{2\mu} \nabla^2 \psi + U\psi = E\psi \quad (21)$$

where  $\mu$  is the reduced mass of the pair,  $E = \hbar^2 k^2 / 2\mu$  is the center of mass energy of relative motion, and  $\psi$  is the stationary scattering wave function, it has to be a sum of a plane wave and of an outgoing spherical wave and satisfies the boundary condition

$$\psi(\mathbf{r}) = e^{ikz} + f(\theta) \frac{e^{ikr}}{r} \quad (22)$$

## Optical model with Partial-wave expansion

In terms of partial-wave radial functions  $y_\ell(r)$ , the complete wave function can be expanded as

$$\psi(\mathbf{r}) = \frac{1}{kr} \sum_{\ell=1}^{\infty} (2\ell + 1) i^\ell y_\ell(r) P_\ell(\cos(\theta)) \quad (23)$$

where  $P_\ell(\cos(\theta))$  are Legendre functions. In the partial-wave expansion method, if the incident beam is unpolarized, the differential elastic cross section is given by

$$\boxed{\frac{d\sigma}{d\Omega} = |f(\theta)|^2} \quad (24)$$



and if the beam is polarized

$$\frac{d\sigma}{d\Omega} = |A(\theta) + B(\theta)|^2 \quad (25)$$

and the polarization vector of the scattered beam along the direction  $\mathbf{n}$  which perpendicular to the scattering plane is

$$\mathbf{P}(\theta) = P(\theta)\mathbf{n} = \frac{A^*(\theta)B(\theta) + A(\theta)B^*(\theta)}{|A(\theta) + B(\theta)|^2} \mathbf{n} \quad (26)$$

where

$$A(\theta) = f_C(\theta) + \frac{1}{2ik} \sum_{\ell=0}^{\infty} e^{2i\sigma_\ell} [(\ell + 1)(S_{\ell, \ell+1/2} - 1) + \ell(S_{\ell, \ell-1/2} - 1)] P_\ell(\cos(\theta)) \quad (27)$$

# OM and eikonal approximation formalism IV

where the right-hand term in brackets is absent for  $\ell = 0$ , the sum on the right is the nuclear phase shift.  $B(\theta)$  is the spin-flip amplitude and it is given by

$$B(\theta) = -\frac{1}{2k} \sum_{\ell=0}^{\infty} e^{2i\sigma_{\ell}} (S_{\ell, \ell+1/2} - S_{\ell, \ell-1/2}) P_{\ell}^{\ell}(\cos(\theta)) \quad (28)$$

The coulomb scattering amplitude is given by

$$f_C(\theta) = \frac{-\eta}{2k \sin^2(\theta/2)} \exp[-i\eta \ln(\sin^2(\theta/2) + 2i\sigma_0)] \quad (29)$$

where  $S_{\ell j} = e^{2i\delta_{\ell j}}$  is the reflection coefficient and  $\delta_{\ell j}$  is the phase shift due to the nuclear and spin-orbit potentials.

$\sigma_{\ell} = \arg\Gamma(\ell + 1 + i\eta)$  is Coulomb phase shift where

$\eta = \mu Ze^2/(\hbar^2 k)$  is the Coulomb or Sommerfeld parameter.

The reaction cross section is given by

$$\sigma_R = \frac{\pi}{k^2(2s+1)} \sum_{\ell=0}^{\infty} \sum_{j=|\ell-s|}^{\ell+s} (2j+1)(1 - |S_{\ell j}|^2) \quad (30)$$

## The eikonal approximation

At high energies, the wave function will oscillate rapidly and the calculation of scattering wave functions for each partial wave becomes more complicated. In the eikonal approximation and the optical limit of the Glauber theory, the wave function can be written as

$$\psi = e^{ikz} \hat{\psi} = \exp\left[ ikz + \frac{1}{i\hbar v} \int_{-\infty}^z U(x, y, z') dz' \right] \quad (31)$$

In the eikonal approximation a straight-line trajectory is assumed. The vector  $r$  is given by  $r = \mathbf{b} + z\hat{z}$  where  $\mathbf{b} = (x, y, 0)$  is called the impact parameter vector. The correspondence between the quantum-mechanical and classical angular momenta,  $\ell + 1/2 = kb$ , is well-known, and it is therefore reasonable to replace the sum over angular momentum  $\ell$  by the integral  $k \int db$ . So the total nuclear reaction cross section is given by

$$\sigma_R = 2\pi \int_0^\infty [1 - e^{2\text{Im}\chi_N(b)}] b db \quad (32)$$

and the elastic differential cross sections as

$$\frac{d\sigma}{d\Omega} = |F(\theta) + G(\theta)|^2 \quad (33)$$

where

$$F(\theta) = f_C(\theta) + ik \int_0^\infty J_0(qb) e^{i\chi_C(b)} \times \{1 - e^{i\chi(b)} \cos[kb \chi_{SO}(b)]\} b db \quad (34)$$

and

$$G(\theta) = ik \int_0^\infty J_1(qb) e^{i\chi_C(b) + i\chi(b)} \sin[kb \chi_{SO}(b)] b db \quad (35)$$

In the equation above,  $q = 2k \sin(\theta/2)$  where  $\theta$  is the scattering angle.  $J_0(J_1)$  is the zero (first) order Bessel function.  $\chi = \chi_N + \chi_C$  where  $\chi_N(b)$ ,  $\chi_C(b)$ , and  $\chi_{SO}(b)$  are the nuclear, Coulomb, and spin phase shift respectively and they can be given by

$$\chi_\tau(b) = \frac{-1}{\hbar v} \int_{-\infty}^{\infty} V_\tau(\sqrt{b^2 + z^2}) dz, \quad \tau \equiv N, C, SO \quad (36)$$

- Microscopic study of proton elastic scattering with helium, lithium, and beryllium isotopes at a wide range of energies start from few MeVs/nucleon up to 200 MeV/nucleon.
- The cross-section data are calculated within:
  - ① The optical model with the partial-wave expansion method.
  - ② The eikonal approximation that based on the Glauber theory.
- The optical potentials is constructed microscopically from the zero-range single-folding model.
- The partial-wave expansion calculation successfully reproduces the scattering observables below 100 MeV.
- At larger energies, some minima appear in  $d\sigma/d\Omega$  and it is resolved by using the eikonal approximation.
- From the parametrization of the calculated volume integrals, a local E-dependent OP is obtained with no fitting parameters.

- This parameterized OP successfully reproduces the scattering data and can be used for energies at which no data exist.
- Study of more data for intermediate and heavy nuclei can lead to get a global microscopic OP.

## Publications

- Eur. Phys. J. A 48, 154 (2012).
- Phys. Rev. C 88, 064602 (2013).
- Eur. Phys. J. WoC 66, 03025 (2014).
- Eur. Phys. J. A 50, 106 (2014).
- Phys. Rev. C 90, 034615 (2014).
- Eur. Phys. J. WoC 107, 08007 (2016).
- AIP Conf. Proc. 1742, 030011 (2016).
- AIP Conf. Proc. 1976, 020004 (2018).

## 2- Extension of the work to 1 GeV I

### Improvements

The spin-orbit OP the derivative of the folding potential  $\Rightarrow$  the microscopic complex spin-orbit OP is taken within Breiva-Rook approximation using spin-orbit NN interaction.

The single-folding potential zero-range  $\Rightarrow$  finite-range exchange part.

NN interaction density-dependent  $\Rightarrow$  the energy-, density-, and isospin-dependent M3Y-paris NN interaction.

Energy range below 200 MeV  $\Rightarrow$  until 1000 MeV.

- The data of the elastic scattering of protons with  ${}^9\text{Be}$  at 3-1000 MeV/nucleon are analysed using the optical model with the partial-wave expansion technique.



## 2- Extension of the work to 1 GeV II

| Data              | Scattering        | Incident energy (MeV/nucleon)   |
|-------------------|-------------------|---|
| $d\sigma/d\Omega$ | $p+{}^9\text{Be}$ | 3, 6, 10, 13, 30.3, 17, 25, 35.2, 49.4, 54.7, 74.7, 100.6,<br>135, 160, 179.9, 201.4, 220, 317, 497.5, 1000 |
| $A_y(\theta)$     | $p+{}^9\text{Be}$ | 8.5, 11.4, 13, 17.8, 30.3, 42, 50, 74.7, 100.6<br>141.5 179.9, 201.4, 220, 317, 497.5, 990                  |

- Goals of the study:

- ① To study the surface contribution at high energies
- ② To determine the energy dependencies of the OP at a wide range of energy.
- ③ To present an E-dependent local microscopic OP which can be used to predict the data at energies where no experimental data are available.
- ④ To test the ability of the folding-model OP with the partial-wave expansion method at high energies.

# The microscopic optical potential I

- The total microscopic optical potential can be rewritten as

$$U_{OP}(r) = N_R V_F(r) + i[N_I W_F(r) - N_{IS} r \frac{d}{dr} W_F(r)] \\ + (N_{SO}^R + iN_{SO}^I) V_{LS}(r) \mathbf{L} \cdot \boldsymbol{\sigma} + V_C(r), \quad (37)$$

- $V_F$  is presented in terms of isoscalar ( $V_{IS}$ ) and isovector ( $V_{IV}$ ) parts. Each term has direct and exchange parts.

$$V_F(\mathbf{r}) = V^D(\mathbf{r}) + V^{EX}(\mathbf{r}) = V_{IS}^D(\mathbf{r}) + V_{IV}^D(\mathbf{r}) + V_{IS}^{EX}(\mathbf{r}) + V_{IV}^{EX}(\mathbf{r}). \quad (38)$$

$$V_{IS(IV)}^D(\mathbf{r}) = \int [\rho_P(\mathbf{r}') \pm \rho_n(\mathbf{r}')] v_{00(01)}^D(\rho, E, s) d^3 r'$$

$$V_{IS(IV)}^{EX}(\mathbf{r}) = \int [\rho_P(\mathbf{r}, \mathbf{r}') \pm \rho_n(\mathbf{r}, \mathbf{r}')] v_{00(01)}^{EX}(\rho, E, s) j_0(k(E, r)s) d^3 r' \quad (39)$$

# The microscopic optical potential II

where  $\mathbf{s} = \mathbf{r}' - \mathbf{r}$ ,  $\mathbf{r}$  is the vector joining the center-of-mass of the target and the incident proton,  $\rho_{\text{p(n)}}(\mathbf{r}, \mathbf{r}')$  is the one-body density matrix for the protons(neutrons) in the target nucleus with  $\rho_{\text{p(n)}}(\mathbf{r}) \equiv \rho_{\text{p(n)}}(\mathbf{r}, \mathbf{r})$ .  $k(E, r)$  is the local momentum of the relative motion determined as

$k^2(E, r) = \frac{2\mu}{\hbar^2} [E_{\text{c.m.}} - V_{\text{F}}(r) - V_{\text{C}}(r)]$  where,  $\mu$  is the nucleon reduced mass,  $E_{\text{c.m.}}$  is the center-of-mass energy.

- To fulfill the saturation of nuclear matter, we use the energy- and density-dependent CDM3Y6 effective Paris interaction as

$$v^{\text{D(EX)}}(\rho, E, s) = g(E)F(\rho)v^{\text{D(EX)}}(s) \quad (40)$$

$$g(E) = 1 - 0.003E, \quad \text{and} \quad F(\rho) = C \left[ 1 + \alpha e^{-\beta\rho(\mathbf{r})} - \gamma\rho(\mathbf{r}) \right],$$

(41)

the GFMC density that based on AV18+IL2 model is used

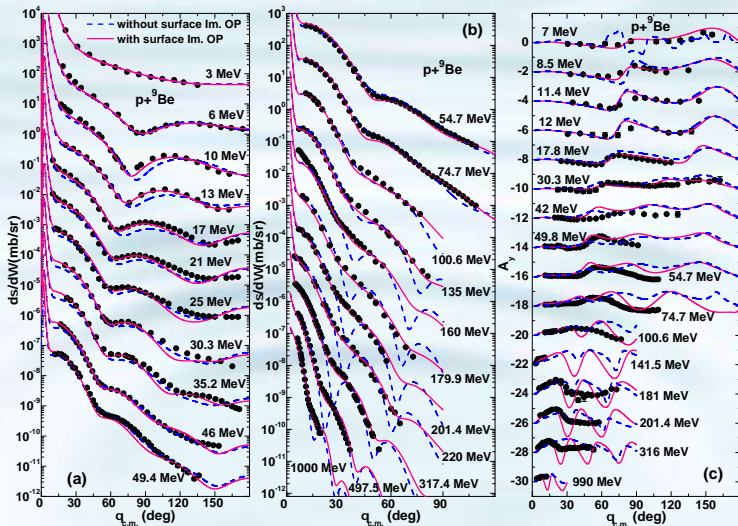
# The microscopic optical potential III

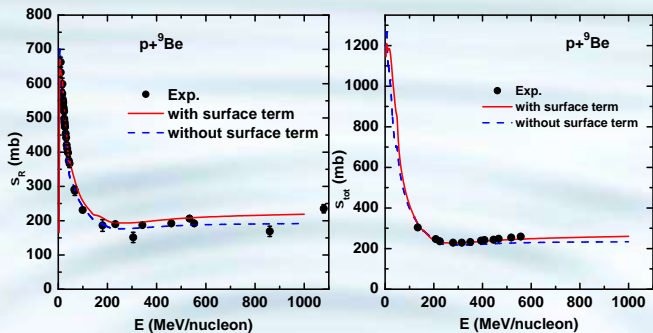
The spin-orbit part of the nucleon-nucleus optical potential  $V_{LS}(r)(\mathbf{L}\cdot\sigma)$  can be evaluated microscopically within Brieva and Rook approximation using the two-body spin-orbit term of M3Y-Paris  $NN$  interaction and the nuclear density of the target as

$$V_{LS}(r) = -\frac{F(\rho(r))}{3} \times \left[ \Phi_p(E, r) \frac{1}{r} \frac{d\rho^p(r)}{dr} + \Phi_n(E, r) \frac{1}{r} \frac{d\rho^n(r)}{dr} \right], \quad (42)$$

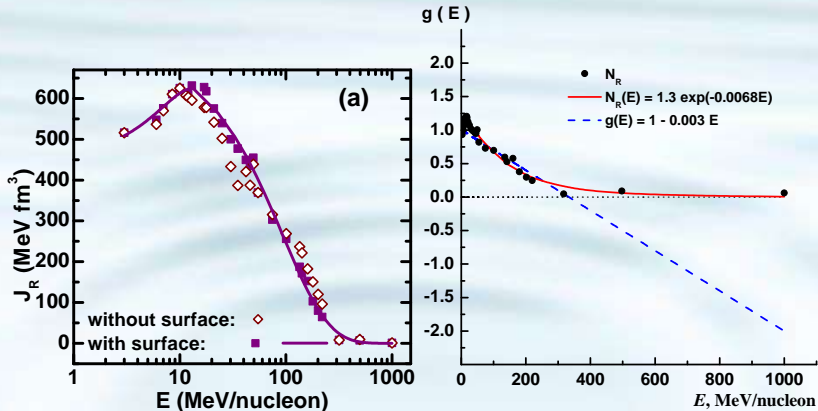
$$\begin{aligned} \Phi_p(E, r) &= \int_0^\infty v_{LS}^{(1)}(s) [1 + \hat{j}_1(k(E, r)s)] s^4 ds, \\ \Phi_n(E, r) &= \frac{1}{2} \int_0^\infty \{v_{LS}^{(1)}(s) [1 + \hat{j}_1(k(E, r)s)] \\ &\quad + v_{LS}^{(0)}(s) [1 - \hat{j}_1(k(E, r)s)]\} s^4 ds. \end{aligned} \quad (43)$$

# Results I

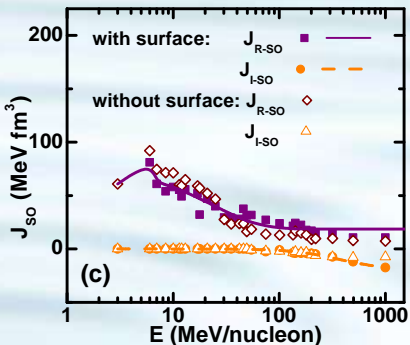
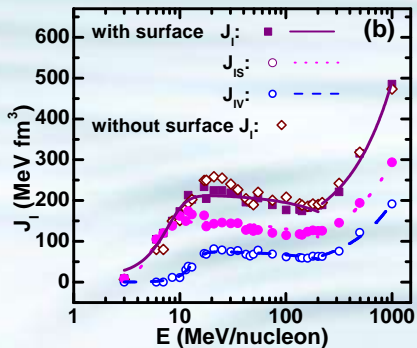




# Energy dependence of the volume integrals I



# Energy dependence of the volume integrals II





# Energy dependence of the volume integrals III

Table: Energy parametrizations of the volume integrals of best-fit potentials. The parameters  $E$  and  $w$  are given in MeV,  $\eta$  in  $\text{MeV}^{-1}$ , and  $J$  in  $\text{MeV fm}^3$ .

| OP part              | Parametrization   | Parameters  |
|----------------------|---|---|
| Real                 | $J_R(E) = \begin{cases} J_R^{(1)} \exp[-(E - E_R)^2/w_R^2] & \text{for } E \leq E_R \\ J_R^{(2)} \exp(-\eta_R E) & \text{for } E \geq E_R \end{cases}$  | $\begin{cases} J_R^{(1)} = 624.0 & w_R = 22.12 \\ E_R = 13 \\ J_R^{(2)} = 721.3 & \eta_R = 0.0107 \end{cases}$  |
| Volume Imaginary     | $J_{IV}(E) = \begin{cases} \frac{J_{IV}^{(1)} - \eta_{IV}^{(1)} E}{1 + \exp(E_{IV} - E)/w_{IV}} & \text{for } E \leq 200 \text{ MeV} \\ J_{IV}^{(2)} + \eta_{IV}^{(2)} E & \text{for } E \geq 200 \text{ MeV}. \end{cases}$ | $\begin{cases} J_{IV}^{(1)} = 76.7 & \eta_{IV}^{(1)} = 0.0977 \\ E_{IV} = 12.5 & w_{IV} = -1.84 \\ J_{IV}^{(2)} = 28.4 & \eta_{IV}^{(2)} = 0.1663 \end{cases}$  |
| Surface Imaginary    | $J_{IS}(E) = \begin{cases} \frac{J_{IS}^{(1)} - \eta_{IS}^{(1)} E}{1 + \exp(E_{IS} - E)/w_{IS}} & \text{for } E \leq 200 \text{ MeV} \\ J_{IS}^{(2)} + \eta_{IS}^{(2)} E & \text{for } E \geq 200 \text{ MeV}. \end{cases}$ | $\begin{cases} J_{IS}^{(1)} = 150.0 & \eta_{IS}^{(1)} = 0.1960 \\ E_{IS} = 5.33 & w_{IS} = -0.94 \\ J_{IS}^{(2)} = 80.2 & \eta_{IS}^{(2)} = 0.2155 \end{cases}$ |
| Real Spin-orbit      | $J_{SO}^R(E) = \begin{cases} J_{SO}^{(R1)} \exp[-(E - E_{SO}^R)^2/w_{SO}^{R2}] & \text{for } E \leq E_{SO}^R \\ A + J_{SO}^{(R2)} \exp(-\eta_{SO}^R E) & \text{for } E \geq E_{SO}^R \end{cases}$                           | $\begin{cases} E_{SO}^R = 6 & w_{SO}^R = 5.62 \\ J_{SO}^{(R1)} = 81.1 & \eta_{SO}^R = 0.0407 \\ J_{SO}^{(R2)} = 58.7 & A = 18.7 \end{cases}$                    |
| Imaginary Spin-orbit | $J_{SO}^I(E) = \begin{cases} 0 & \text{for } E \leq 50 \text{ MeV} \\ J_{SO}^I \frac{E^2}{E^2 + w_{SO}^I} & \text{for } E \geq 50 \text{ MeV}. \end{cases}$   | $\begin{cases} J_{SO}^I = -19.2 & w_{SO}^I = 365 \end{cases}$   |

$$\begin{aligned}
 U_{OP}(r, E) = & N_R(E)V_F(r) + i[N_I(E)W_F(r) \\
 & - N_{IS}(E)r\frac{d}{dr}W_F(r)] \\
 & + [N_{SO}^R(E) + iN_{SO}^I(E)]V_{LS}(r)\mathbf{L}\cdot\boldsymbol{\sigma} + V_C(r),
 \end{aligned} \tag{44}$$

$$\begin{aligned}
 U_{OP}(r, E) = & \frac{J_R(E)}{J(V_F)}V_F(r) + i\frac{J_{IV}(E)}{J(W_F)}W_F(r) \\
 & - i\frac{J_{IS}(E)}{J(-rdW_F/dr)}r\frac{d}{dr}W_F(r) \\
 & + \left[ \frac{J_{SO}^R(E)}{J(V_{LS})} + i\frac{J_{SO}^I(E)}{J(V_{LS})} \right] V_{LS}(r)\mathbf{L}\cdot\boldsymbol{\sigma}.
 \end{aligned} \tag{45}$$

# Conclusions

- The partial-wave expansion analysis fails to reproduce  $d\sigma/d\Omega$  data at energies larger than 100 MeV.
- A good improvement is obtained by including the surface imaginary contribution at high energies where most of the basic scattering observables ( $d\sigma/d\Omega$ ,  $A_y$  and  $\sigma_R$ ) are reproduced well at the considered wide energy range.
- The volume integrals parameterizations are used to build an energy-dependent microscopic OP that used to reproduce the observables at a wide energy range until 1 GeV.
- This study shows that the partial-wave expansion analysis using the folding optical model can be used to analyse the scattering data at high energies as well as at low energies.

## new Publications

- H. M. Maridi, *Phys. Rev. C*, 100, 014613 (2019).
- H. M. Maridi, *Bull. Russ. Acad. Sci. Phys.* 84, 473 (2020).

Thank you